INTERNATIONAL JOURNAL OF HYDROGEN ENERGY XXX (2017) 1–12

Available online at www.sciencedirect.com

ScienceDirect

journal homepage: www.elsevier.com/locate/he

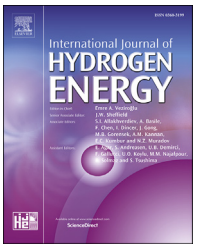

Enhanced photocatalytic activity of Pt deposited on titania nanotube arrays for the hydrogen production with glycerol as a sacrificial agent

Slamet [a], *Ratnawati* [b,*], *Jarnuzi Gunlazuardi* [c], *Eniya Listiani Dewi* [d]

[a] *Department of Chemical Engineering, Faculty of Engineering, Universitas Indonesia, Depok 16424, Indonesia*
[b] *Department of Chemical Engineering, Institut Teknologi Indonesia, Tangerang Selatan 15320, Indonesia*
[c] *Department of Chemistry, Faculty of Mathematics and Sciences, Universitas Indonesia, Depok 16424, Indonesia*
[d] *Agency for the Assessment and Application Technology, Puspiptek, Serpong, Tangerang Selatan 15320, Indonesia*

ARTICLE INFO

Article history:
Received 30 May 2017
Received in revised form
18 July 2017
Accepted 26 July 2017
Available online xxx

Keywords:
Titania nanotube arrays
Platinum
Chemical reduction
Photo-assisted deposition
Hydrogen

ABSTRACT

Photocatalytic activity of Pt-loaded TiO_2 nanotube arrays (Pt-TNTA) in the presence of glycerol as a sacrificial agent to produce H_2 has been studied. The effects of Pt loading and the methods by which it is deposited on TNTA (chemical reduction and photo-assisted deposition) were carefully examined. Intermediate products were also identified in order to scrutinise the reaction pathways of hydrogen generation in this particular system. FESEM imaging confirmed the formation of nantotubular structures of TiO_2 with average inner diameter of 80 nm, wall thickness of 20 nm, and length of approximately 2.5 μm. The generated nanotube arrays were of anatase structure with crystallite size within the range of 22–30 nm. Pt was successfully deposited on the surface of TNTA, as corroborated by EDX spectra, elemental mapping and TEM analysis. Band gap narrowing upon Pt loading was implied by UV–Vis DRS analysis, resulting in a band gap value of 2.93 eV, notably lower than a typical value of 3.2 eV associated with anatase. The photocatalyst sample with Pt deposited via a photo-assisted deposition method (Pt-TNTA-PDC) evidently outperformed its bare TNTA counterpart in producing hydrogen by 4.7 times, while that with Pt deposited by chemical reduction could improve H_2 production by 3.8 times. During photocatalytic operations, glycerol served an important purpose in suppressing electron-hole recombination by providing holes an oxidative target which is less energy-demanding than water. It is proposed that glycerol underwent dehydrogenation and decarbonylation processes producing ethylene glycol, followed by dehydration and oxidation towards acetic acid, before transforming into H_2 and CO_2, eventually. We suggest that Pt plays a role not only in the enhancement of H_2 photoproduction, but also in governing the direction of reactions, hence the intermediates and final products.

* *Corresponding author.*
E-mail address: rnwt63@yahoo.co.id (Ratnawati).

http://dx.doi.org/10.1016/j.ijhydene.2017.07.208

Introduction

Utilizing solar energy with TiO_2-mediated photocatalytic reactions have been studied extensively in the last decade especially for production of renewable energy like H_2 [1–9] on the purpose of responding to the ever increasing energy demand as well as circumventing the inevitable depletion of fossils fuels and environmental pollution [10]. To date, nearly 95% of H_2 in the market was produced via conventional technology, such as methane steam reforming and pyrolysis which are generally energy demanding, while offering low H_2 selectivity [7–11]. It is therefore imperative to assemble advanced H_2 generation systems, namely utilizing renewable sources, such as water or biomass, and implementing a cost effective process, such as photocatalysis. In fact, many biomass feedstocks such as methanol, ethanol, glycerol [9,12], or many organic pollutants can be integrated into a photocatalytic reaction system as anodic sacrificial agents, hence kinetically enhancing H_2 production while eliminating pollutants at the same time [5,6,8,13,14]. In this process, photosplitting of water and photo-reforming of sacrificial agents are believed to take place simultaneously in the absence of oxygen. Introducing sacrificial agents, being from inorganics (H_2S, S^{2-}/SO_3^{2-}, Fe^{2+} etc) or organics (alcohols, acids, aldehydes, sugar etc) into a photocatalytic system is known to be an effective way to suppressing electron-hole recombination. H_2 yield is significantly improved as the sacrificial agents are oxidized by holes, •OH radicals, and/or oxygen produced by cleavage of water [8–11,15,16]. Furthermore, this arrangement also results in the suppression of O_2–H_2 back reaction [7,8]. The affinity of these agents towards holes would depend upon their polarity, which in turn affects their adsorptive properties on photocatalyst surface [15]. One of the most intriguing sacrificial agents is glycerol because it is considered as a biodegradable, nontoxic, and, nonflammable substrate. Being an undesired by-product in biodiesel industry, the demand for glycerol is relatively limited, so to many it is regarded as waste [10]. Therefore, this would be beneficial as a new avenue for H_2 generation and waste limitation.

Among other light-harvesting semiconductors, TiO_2 is the most studied material and widely considered as the most promising photocatalyst due to its cost effectiveness, nontoxicity, low environmental impact, high photocatalytic activity [6,17–20] and excellent stability (in alkaline and acidic solution as well as under illumination) [21]. The versatility of TiO_2 as a photocatalyst is proven by its wide applications, which include air and water purifications (removal of organic and inorganic pollutants [19,22], photo-driven disinfection of pathogenic micro-organisms as viruses and bacteria [22,23], self-cleaning, self-sterilizing, anti-fogging [19,21], and dye-sensitized solar cells [25]. Compared to others morphologies (nanorods, nanotube, nanowires, nanobelt), well aligned TiO_2 nanotube arrays (TNTA) produced from anodic oxidation of Ti foil are favored in many cases, owing to its tunable structure, effective photon absorption, and extensive internal surface area [20,21,25,26]. However, its applications have been constrained by rapid recombination of photogenerated electron-hole pairs, inactivity under visible, and large overpotential for H_2 generation [1–6,16,17,19–21,24–27]. This is because, photo-generated electrons and holes resulted by photocatalysis can either react with adsorbed species or undergo undesired recombination [10]. Tremendous efforts have been performed to narrow the band gap in order to enhance the visible light response, including incorporating non-metal doping (C, N, B, and F) to the matrix of TNTA, and coupling with low-band-gap semiconductors such as CdS, CdSe, PbS or WO_3 [1–4,19,24–27]. In order to hamper the fast recombination of photogenerated electron-hole pairs, deposition of high-work-function metals such as Pt, Au, Pd, Ni, Cu, Rh and Ag on TiO_2 have been previously reported to be a useful approach [5,7–9,11,12,20,21,25,26,28,29]. Enhancement of photocatalytic activity can also be performed by the use of TiO_2–Co_3O_4–Pt and TiO_2/WO_3/Pt since co-catalyst Co_3O_4–Pt can suppress recombination and provide extensive active sites [30], while WO_3 and Pt can act as hole and electron collectors, respectively [1]. Branched hydrogenated TiO_2 has also been reported effective to promote the separation of electron-hole [17]. In addition, incorporation of $Cu_2(OH)_2CO_3$ onto TiO_2 also enhanced the water splitting reaction as reported by He at al [31]. Meanwhile, direct Z-scheme anatase/rutile TiO_2 nanofiber photocatalyst could also enhance photocatalyst efficiency in H_2 production [18].

Increasing attention has been devoted to Cu_2O, CuO, CuO_x that embedded on TiO_2 [11,12,16,31] to enhance H_2 production since these metal oxides are abundant, cheaper, non-toxicity, very active and their bandgaps are suitable for water splitting [11,12]. However, formation of partially oxidized species strongly adsorbed on the surface can lead to deactivation. Moreover, the presence of complexing agent, such as carboxylic acids can lead to the leaching of highly disperse metals. Some researchers also reported that Cu leaching is observed under visible light irradiation and it can be minimized by UV back photodeposition [10,12,16]. On the other hand, Pt is one of the noble metals that occupy the largest work function (5.65 eV), low overpotential for solar harvesting fuel generation [1], and has higher stability compared to others [25]. Therefore, it performed better as electron trapper [5,20–22,25]. When Pt is deposited on TNTA, the formation of Schottky barriers at the interface between TNTA and Pt occurs, hence, the photogenerated electron can be captured easily [5,28]. The availability of Pt on TNTA not only reduce the recombination the photogenerated electron-hole pairs but also modified Pt-TNTA utilizes visible light effectively [15,28,29]. However, the price of this metal is expensive among others [8], therefore the selection of the appropriate method in depositing Pt on TiO_2 is necessary to get the optimum Pt-depositing amount. Recently, various methods have been reported for the preparation depositing Pt on the TiO_2, including impregnation Pt on TiO_2 nanoparticles (TNP) for hydrogen production [14,15], ion-exchange and incipient wetness Pt on TiO_2 nanotube non-arrays (TNT) for water splitting [29], ion sputtering Pt on TNTA for fuel cell [32], dipping and deposition Pt on TNTA [33], modified photo irradiation-reduction Pt on TNTA for degradation of Rhodamine B [25], hydrogen reduction Pt on TNTA [21], electrodeposition Pt on TNTA for methanol oxidation [34], photo-assisted deposition (Pt on TNP for hydrogen production from methanol solution) [35], Pt on TNT for degradation of methyl orange [28], Pt on TNTA for water splitting [20] and chemical reduction Pt on TNT for hydrogen

Please cite this article in press as: Slamet, et al., Enhanced photocatalytic activity of Pt deposited on titania nanotube arrays for the hydrogen production with glycerol as a sacrificial agent, International Journal of Hydrogen Energy (2017), http://dx.doi.org/10.1016/j.ijhydene.2017.07.208

generation from ethanol solution [5]. From above methods, chemical reduction and photo-assisted deposition are excellent methods and have several advantages over other methods in term of high yield, high dispersion, etc as reported by Anthony et al. and An et al. [5,28]. In addition, photodeposition is the most commonly technique in depositing metals on TiO_2 and involves the metal ions reduction by electrons and the oxidation of water by holes. Improvement the rate of photodeposition can be obtained by addition of acetate, formaldehyde, and methanol [22]. However, to the best of our knowledge, the comparison of Pt deposited on TNTA via chemical reduction and photo-assisted deposition methods especially its application on the hydrogen generation with glycerol (the by-product of the biodiesel industry) as a sacrificial agent still remain substantially missing.

In the presents study, the effects of relevant parameters on the rate of hydrogen generation are investigated, including the amount of Pt loading and the methods by which the deposition was conducted (chemical reduction with NaBH4 as reducing agent and photo-assisted deposition). The synthesized materials were probed by FESEM-EDX, TEM, UV–Vis DRS, AAS and XRD. Intermediates and final products from the H_2 generation operations were identified on the purpose of predicting the mechanism by which glycerol is consumed in a photocatalytic system containing a solution of water-glycerol mixture (10 v% glycerol which represents its concentration in the biodiesel waste). The photon source used irradiates predominantly visible light (83%) in order to approximate the solar light.

Experimental

Synthesis of TNTA

Anatase TiO_2 nanotube arrays (3 × 3 cm) were synthesized by anodization process of titanium sheet in 60 ml of glycerol electrolyte solution containing 0.5 wt% NH_4F and 25 v% H_2O. A constant potential of 30 V was set using DC power supply (Escord 6030SD) for 90 min anodization under ultrasonic waves (Telsonic TPC 015, 200 W, 65 kHz) instead of magnetically stirring at 50 °C according to the maximum temperature achieved during sonication. The selection of constant parameters such as voltage, water content, the amount of NH_4F and annealing temperature is based on the optimal condition in our previous studies [6]. Details anodization technique has been explained as previously reported [6]. In the preliminary experiment, anodization time was varied (10; 30; 60; 90 and 150 min) and based on the morphology of TNTA synthesized, 90 min anodization performed the optimum condition with the longest and ordered nanotubes, and therefore, it is selected for the following study. After finishing anodization, amorphous TNTA were then annealed at 500 °C for 3 h to crystallize them.

Deposition of Pt on TNTA (Pt-TNTA)

Platinum nanoparticles were deposited on TNTA via chemical reduction and photo-assisted deposition methods. For the chemical reduction method, amorphous TNTA were dipped in the 60 ml solution that contains 0; 3; 9; 15; and 24 ppm of Pt (H_2PtCl_6 as the precursor) and followed by addition of the excess of $NaBH_4$ under stirring. After 1 h chemical reduction reaction, the Pt-TNTA were then washed repeatedly with distilled water and ethanol (denote as Pt-TNTA-CRA). Subsequently, the samples were annealed to crystallize them under 20% H_2 in an argon atmosphere (150 ml/s) at 500 °C for 3 h with the heating rate of about 9 °C min^{-1} and cooling naturally. Pt deposited on annealed (crystallized) TNTA with chemical reduction method was also performed by dipping it in the 60 ml solution that contains 15 ppm of Pt (denote as Pt-TNTA-CRC). For the photo-assisted deposition method, crystallized TNTA were placed in the photoreactor that contains 60 ml solution (10 v% methanol with 15 ppm of Pt). This process was carried out for 6 h under magnetically stirred, illuminated with 6 lamps of UV-A (@15 W) in the Pyrex glass reactor that placed inside the reflection box. After photo deposition, Pt deposited TNTA was rinsed repeatedly with distilled water and followed by drying at 130 °C for 1 h in the furnace (denote as Pt-TNTA-PDC). In all annealing processes, a similar procedure was performed). These photocatalysts were then used to produce hydrogen.

Characterization of Pt-TNTA

The morphological analysis of the Pt-TNTA was done by Field Emission Scanning Electron Microscope, FESEM (FEI-Inspect F50 and Jeol-JIB-4610F) and Transmission Electron Microscope, TEM (FEI type, Tecnai G2 STWIN, 200 kV). Energy dispersive X-ray analyzer (EDX, Oxfords XMAX 50 detector) is attached to the FESEM to determine the composition of the samples. To measure the energy band gap of the samples that result of the Pt deposited on TNTA, a UV–Vis DRS analysis was employed using Spectrophotometer Shimadzu 2450 type in the wavelength range of 200–600 nm. The crystalline phases of the samples were identified using Shimadzu XRD 7000 X-ray diffractometer with the scan rate at 2° min^{-1} over the 2θ range of 10–80° and it was operated at 40 kV and 30 mA. The source of the X-ray radiation was Cu Kα (λ = 0.154184 nm). The crystallite sizes of the samples were estimated from FWHM (full-width at half-maximum) of XRD by the Scherrer equation. The real Pt deposited on prepared Pt-TNTA were measured using Atomic Absorption Spectroscopy (AAS Annalyst 400 type, Perkin Elmer).

Final and intermediate products identification

Final and Intermediate products identification from the photocatalytic reaction of water-glycerol solution to produce hydrogen were carried out using an experimental setup that consists of a 500 ml Pyrex glass reactor equipped with the thermocouple, magnetic stirrer, a mercury lamp that consist of 83% of the visible and 17% of UV light (Philips HPL-N 250 W/542 E40 HG ISL) that placed inside a reflector box. The schematic of the experimental setup similar to the paper that previously reported [6]. Before starting the experiments, the reactor was flushed with argon and magnetically stirred for about 30 min. At regular time interval, the products generated was analyzed by on-line sampling using Shimadzu Gas Chromatograph (GC 2014) equipped with the Molecular sieve

Please cite this article in press as: Slamet, et al., Enhanced photocatalytic activity of Pt deposited on titania nanotube arrays for the hydrogen production with glycerol as a sacrificial agent, International Journal of Hydrogen Energy (2017), http://dx.doi.org/10.1016/j.ijhydene.2017.07.208

(MS Hydrogen 5A, 80–100 mesh) and CO_2 Porapack N packed columns (L = 6 m, Di = 2.2 mm) with Thermal Conductivity Detector (TCD) to record the peak of H_2, O_2 and CO_2 generated with Ar as a carrier gas. Meanwhile, Gas Chromatograph with Flame Ionization Detector (FID) Shimadzu GC 2014 with RTX-capillary column (L = 30 m, Di = 0.25 mm) is used to analyze the intermediate products in the liquid and gas phase with He as a carrier gas. The GC is interfaced to a personal computer that at time intervals can detect the peak of samples. These intermediate products are confirmed by injection of the standard solution that at certain retention time could detect the certain compound. Identification and quantification were performed at desired time. This GC system equipped with GC solution software that can detect the area of peaks below 50 counts.

Results and discussion

Effect of Pt loading

Fig. 1 presents accumulative H_2 generation on Pt-TNTA-CRA as a function of irradiation time for various photocatalysts with difference Pt loading in TNTA. The uses of Pt-TNTA- CRA with 0, 3, 9, 15, and 24 ppm Pt loading (concentration during preparation) produce 66, 146, 196, 249, and 221 mmol/m^2 photocatalyst, respectively.

The excess of $NaBH_4$ as the reducing agent could reduce Pt^{4+} to Pt^o. In this process, the color of the solution changed from white to black which indicated that Pt has been reduced to Pt^o and readily deposited on TNTA surface. From Fig. 1, it is clear that the H_2 generation is enhanced by loading of Pt up to 15 ppm in the solution (as the optimum condition) while the photoactivity declined in the case of 24 ppm Pt concentration. At higher concentration than its critical point, Pt tends to behave as a promotor of recombination center, providing the activation sites of the charge carriers, since there is no vacant sites left on the TNTA for Pt to occupy [14,22,29,36]. Another reason is, at high loading, a cluster of Pt (agglomeration) is formed, resulting in low dispersion or interface surface area shrinkage [5]. Considering the reduction of H^+ to H_2 on Pt is a surface reaction, H_2 production is expected to diminish due to this effect. A similar result was also reported by Anthony et al. [5] when they studied the significance of Pt loading on powdered TNT with chemical reduction method. Excessive Pt loading can cause a so-called shielding effect that reduces the photon absorption on the surface of Pt-TNTA [14,22]. In addition, metal loadings above its optimum values decrease in electron density occurs because of electron attraction by great quantities of metal. This condition result in complicated field configuration that disturbs charge separation hence interfering with photocatalytic process [22]. H_2 generated from Pt-TNTA-CRA 15 ppm was the highest, 3.8 times higher as compare to the bare TNTA which is attributable to the role of Pt as an electron trapper that dissipates electron-hole recombination. Moreover, Pt loaded on TNTA could lower hydrogen over potential and avoid back reaction of H_2 and O_2 to become water. Pt is also known as an oxidation catalyst that participated in catalyzing glycerol oxidation [14]. For the following experiments, the Pt loading was used 15 ppm, since it exhibit the optimum photoproduction of H_2.

FESEM micrographs of the TNTA and Pt-TNTA-CRA at 15 ppm Pt loading is presented in Fig. 2. Irregularities of the tube length were observed. This may be attributed to the fact that no stirring was applied during synthesis, although sonication aided the process, which is similar with our previously published method [37]. Micrographs presented in Fig. 2 confirmed the formation of nantotubular structures of TiO_2 with average inner diameter of 80 nm, wall thickness of 20 nm, and length of approximately 2.5 μm. Although Pt nanoparticles were not visible in the FESEM images, EDX and elemental mapping results indicated the presence of Pt (Fig. 3). This phenomenon is in accordance with the study reported by previous researchers in which Pt dispersion is not observed in the FESEM image but it is confirmed by EDX [5]. Pt deposited on TNTA was observed in the FESEM image if the Pt formed the agglomeration on the mouth of tubes [32] and if it is not, Pt was spread evenly. Otherwise, decorating Pt on TNTA can be seen using TEM characterization [5,21]. Fig. 2 shows that the tubular morphology is not destructed by depositing Pt on TNTA, which is in agreement with previously publish report [15]. The effect of deposition methods on the resultant

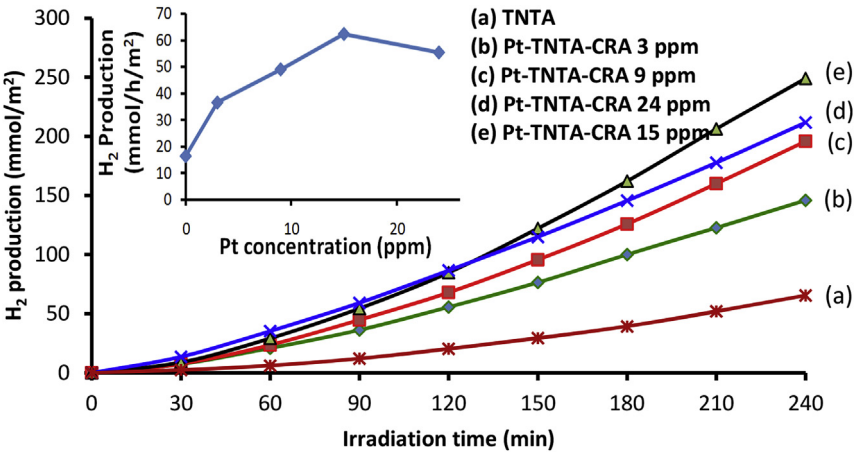

Fig. 1 – Accumulative H_2 production of various Pt-TNTA-CRA with different Pt loading as a function of time. The inset shows H_2 production rate as a function of various Pt loading.

Please cite this article in press as: Slamet, et al., Enhanced photocatalytic activity of Pt deposited on titania nanotube arrays for the hydrogen production with glycerol as a sacrificial agent, International Journal of Hydrogen Energy (2017), http://dx.doi.org/10.1016/j.ijhydene.2017.07.208

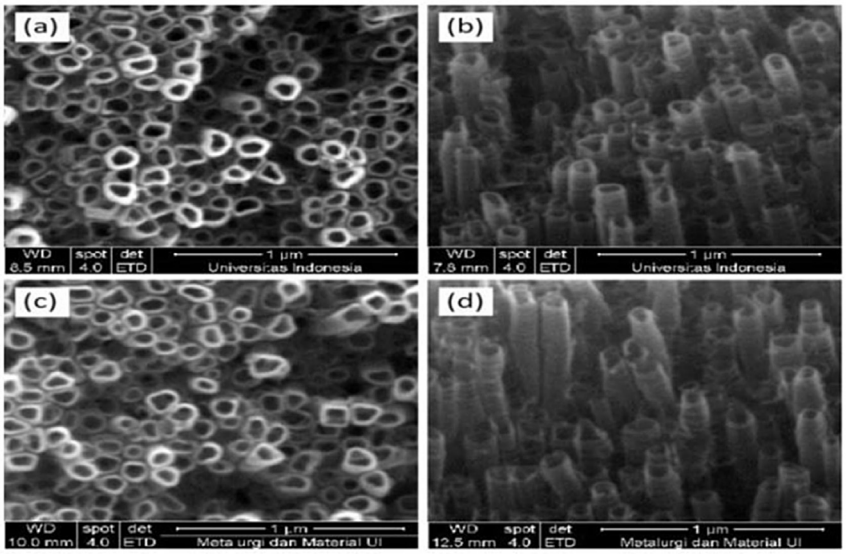

Fig. 2 – FESEM (a) Top image, (b) with angle 45° of TNTA, and (c) Top image, (d) with angle 45° of Pt-TNTA-CRA at 15 ppm Pt loading.

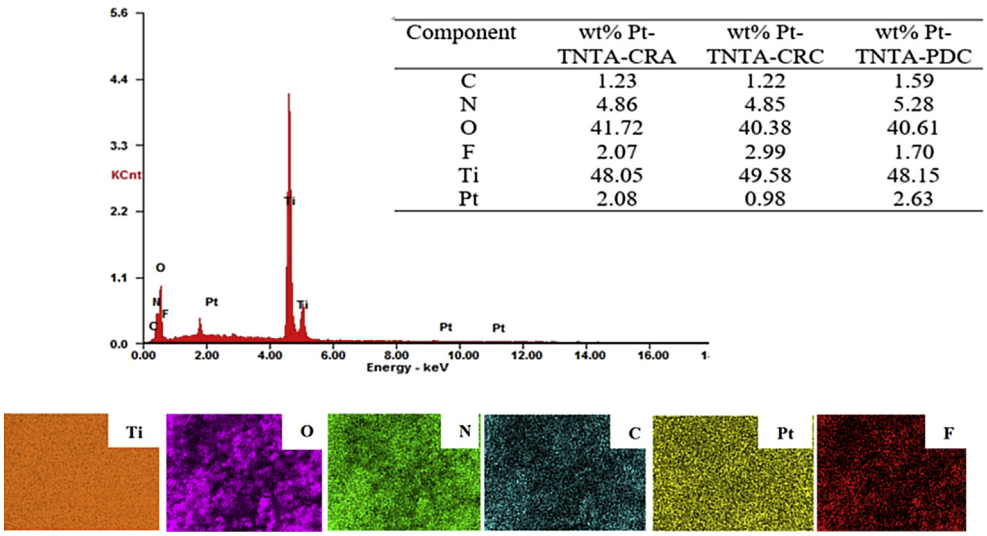

Component	wt% Pt-TNTA-CRA	wt% Pt-TNTA-CRC	wt% Pt-TNTA-PDC
C	1.23	1.22	1.59
N	4.86	4.85	5.28
O	41.72	40.38	40.61
F	2.07	2.99	1.70
Ti	48.05	49.58	48.15
Pt	2.08	0.98	2.63

Fig. 3 – EDX and elemental mapping analysis of the Pt-TNTA.

elemental composition (average values of 3 different areas) on TNTA surface is represented in the EDX spectra and mapping depicted in Fig. 3. Nonmetal C, N, and F were expectedly observed in the elemental analysis and mapping of Pt-TNTA since they incorporated into the matrix of TNTA via in-situ anodization, as reported in our previous study [6]. Fig. 3 presents Pt deposited on the TNTA using TEM characterization. It is obvious that the Pt particles in the Pt-TNTA-PDC are well disperse. The Pt particles in the TEM appear as a black dots as the electron density of the Pt is higher compared to the TiO_2. The TEM result is consistent with the results of EDX and elemental mapping (see Figs. 3 and 4).

The band gap energy of the photocatalyst was estimated by the Kubelka- Munk function and Tauc plot [38] as can be seen in Fig. 5. The band gap narrowing of TNTA down to 3.09 eV (from the original anatase band gap of 3.2 eV) was mostly ascribed to the incorporation of C and N in the matrix of TNTA (Fig. 3 inset) during anodization. This is due to the fact that the electrolyte used during synthesis contained glycerol and NH_4F as sources of carbon and nitrogen atoms, respectively [6]. It appears that decoratin Pt on the surface of TNTA could further reduce the band gap to 2.93 eV. The presence of Pt in the photocatalyst system allows trapping of conduction band electrons upon excitation. The interfacial interaction between TNTA and a highly electronegative metal such as Pt leads to a shift of the Fermi level of TNTA towards its conduction band. This phenomenon could be the underlying reason behind the band gap narrowing of TNTA. Similar results have also been reported by other authors wherein the optical absorption within the visible light region is observed upon depositing Pt

Please cite this article in press as: Slamet, et al., Enhanced photocatalytic activity of Pt deposited on titania nanotube arrays for the hydrogen production with glycerol as a sacrificial agent, International Journal of Hydrogen Energy (2017), http://dx.doi.org/10.1016/j.ijhydene.2017.07.208

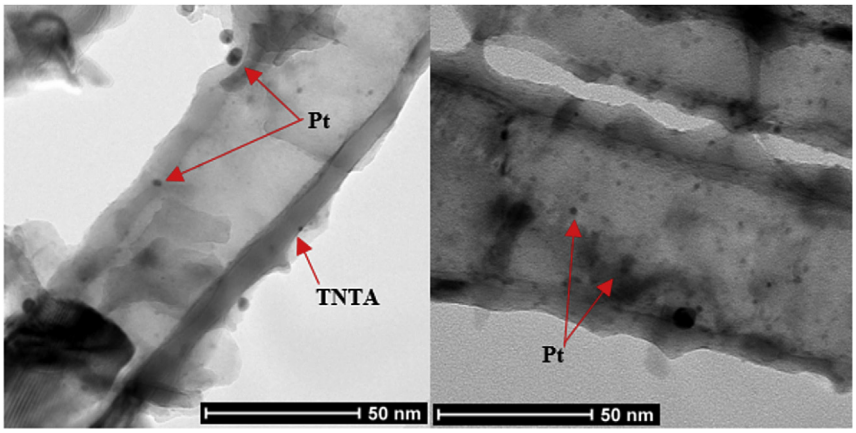

Fig. 4 – TEM image of Pt-TNTA-PDC.

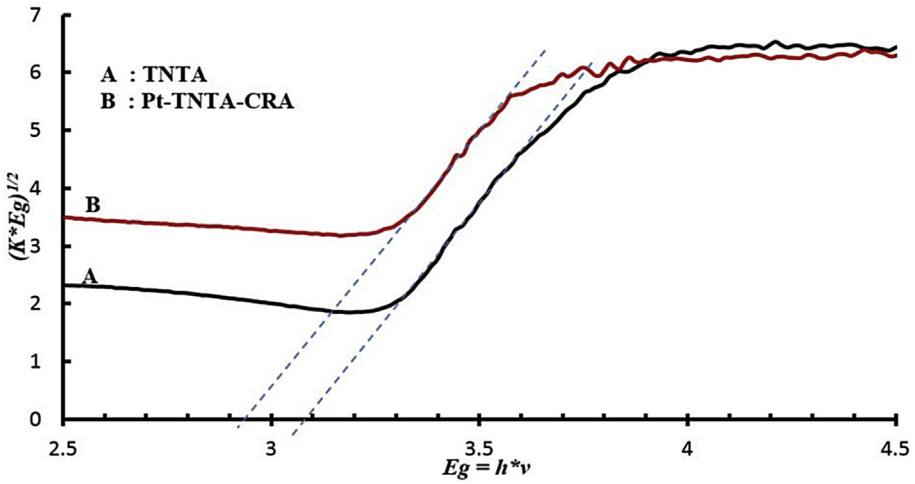

Fig. 5 – Tauc plot of transformed Kubelka-Munk function vs energy (eV) for (a) TNTA and (b) Pt-TNTA-CRA 15 ppm.

on TiO_2 [13,28–30]. The presence of metal nanoparticles on TiO_2 system that have surface plasmon resonance bands can also enhance visible light absorption [10].

Effect of Pt depositing methods

The deposition process of Pt on TNTA via chemical reduction method is according to the reaction in Eq. (1) [5], while for the photo-assisted deposition method is shown in Eq. (3) [28]:

$$NaBH_4 + H_2PtCl_6 + 3H_2O \rightarrow Pt + H_3BO_3 + 5\,HCl + NaCl + 2H_2 \quad (1)$$

$$TiO_2\,(h\upsilon) \rightarrow TiO_2\,(e^- + h^+) \quad (2)$$

$$PtCl_6^{-2} + 4e^- \rightarrow Pt + 6Cl^- \quad (3)$$

According to Eq. (1), when the reducing agent ($NaBH_4$) was added, the solution changed to alkaline as the pH increased to around 9. According to AAS analysis, the real Pt deposited on prepared Pt-TNTA-PDC (4.21 ppm) showed the higher compared to the Pt-TNTA-CRA (3.17 ppm). The AAS data were in a good agreement with the EDX result as shown in Fig. 3 inset that Pt deposited on Pt-TNTA-PDC is greater compared to the Pt-TNTA-CRA. This is likely due to the difference in reaction time: the photo-assisted deposition was carried out for 6 h while the chemical reduction was conducted in only 1 h. However, although the latter is operated in much shorter time than the former, the resultant Pt content in both cases was close enough to perform comparative investigation (2.63 wt% in TNTA-PDC and 2.08 wt% Pt in TNTA-CRA). In addition, Pt deposition is expected to favor the photo-assisted deposition method because the reduction of Pt (from Pt^{4+} to Pt^0) takes place right on the surface of TNTA (Eqs. (2) and (3)), while in the case of $NaBH_4$-driven reduction, the reduction occurs on the bulk solution (Eq. (1)). In the latter case, mass transfer is required for the reduced Pt to be attached on TNTA surface. From Fig. 3 (inset), Pt deposited on amorphous TNTA (Pt-TNTA-CRA, 2.08 wt%) exhibit significantly different behavior as compared to the Pt deposited on crystalline TNTA (Pt-TNTA-CRC, 0.98 wt%). This is because the surface of amorphous TNTA is populated by hydroxyl groups due to the

Please cite this article in press as: Slamet, et al., Enhanced photocatalytic activity of Pt deposited on titania nanotube arrays for the hydrogen production with glycerol as a sacrificial agent, International Journal of Hydrogen Energy (2017), http://dx.doi.org/10.1016/j.ijhydene.2017.07.208

fact that this surface has greater water content [39]. In our previous study, FTIR analysis indicated that the absorption intensity of amorphous TNTA at around 1630 cm^{-1} that correspond to the bending vibration mode of O–H bond of surface adsorbed water molecules is higher as compared to the crystallite TNTA (data not presented) [40]. Since Pt in its ionic form is soluble in water, its penetration onto the surface of amorphous TNTA is favored than that onto the crystallite TNTA. As a result, the amorphous phase of TNTA favors the deposition of Pt as compared to the crystalline one. In addition, the surface area of the amorphous TiO_2 is two times higher than that of crystalline TiO_2 [41], hence providing more sites for Pt deposition. Since the Pt-TNTA-CRA has slightly different in term of the Pt deposited compared to the Pt-TNTA-PDC, chemical reduction method for depositing Pt on amorphous TNTA could be proposed as an alternative and effective method.

Fig. 6 depicts the XRD pattern of the various photocatalysts. XRD result indicated that depositing Pt on TNTA could increase degree of crystalline and crystallite size assigned with the increasing intensity and narrowing the FWHM. For all photocatalysts, the peaks in 2θ at 25.3°, 37.9°, 48.04°, 54.04°, 55.09° which represented the diffraction in the field of (101), (004), (200), (105), (221) were the TNTA anatase phase (JCPDS No.21-1272) [30]. On the basis of calculation using Scherrer formula [5,31,42], the peak intensity at 25.3° corresponds to crystallite size of 20, 22, 28, and 30 nm for TNTA, Pt-TNTA-CRC, Pt-TNTA-PDC, and Pt-TNTA-CRA respectively. It appears that Pt content on TNTA has a positive correlation with the degree of crystallinity and crystallite size. This phenomenon is attributed to the location and incorporation of Pt in the lattice of TNTA [43] or may also be an indication for the slight lattice distortion in the structure of Pt-TNTA. Among Pt-TNTA samples, the diffraction peak of Pt-TNTA-CRC, which represents the degree of crystallinity is the lowest with the smallest crystallite size (22 nm). The omission of Pt in the diffraction patterns could be an indication of the uniform dispersion of Pt nanoparticles or insufficient amount of Pt crystals [1,8,15,28,36]. Pt diffraction peak could have been observed at 2θ of 39,7°, corresponding to a (111) Pt crystal if the amount of Pt is adequate (more than 5 wt% in TNT) [5]. Job et al. reported that Pt diffraction peaks are observable at 2θ of 39,7° and 46,2° for Pt loading of 7.5 wt% [44].

Hydrogen generated by various Pt depositing method is presented in Fig. 7. Obviously, the photocatalytic performance is significantly enhanced when Pt is deposited on TNTA. Pt can collect electrons then reduce H^- to H_2, and holes can oxidize glycerol more easily than water, and therefore, recombination can be reduced [11]. The Pt-TNTA-PDC exhibited the highest H_2 generation (312 mmol/m^2) which 1.3 times compared to the Pt-TNTA-CRA (249 mmol/m^2), 3.1 times compared to Pt-TNTA-CRC (100 mmol/m^2) and 4.7 times compared to bare TNTA (66 mmol/m^2). H_2 production of the Pt-TNTA-PDC is highest since it performed the highest Pt content/deposited (EDX and AAS analysis) and from the XRD analysis, it has better the degree of crystalline. Since the Pt-TNTA-PDC performed the highest Pt content as well as H_2 production, meant that Pt is dispersed evenly. The more the Pt deposited until the optimum condition, the more the H_2 generated since more electrons were trapped by Pt, and therefore hampered the recombination of electron-hole pairs. The amount of Pt deposited on the TNTA-CRA (2.08 wt%) is higher than on the TNTA-CRC (0.98 wt%). As a result, this photocatalyst gave better activity in generating hydrogen. For three types of Pt-TNTA, hydrogen generated has a direct correlation and proportional with the Pt content on the TNTA. The more the Pt deposited on the Pt-TNTA that describes high Pt-reduction efficiency on the TNTA, the more H_2 generated. This condition could give an indication that Pt spread evenly or performed the high degree of dispersion.

To give evidence that loading Pt 15 ppm in the solution via photo-assisted deposition method (Pt-TNTA-PDC) gave optimum condition, 24 ppm Pt loading via this method is also performed and the result indicated that this photocatalyst produced H_2 smaller (230 mmol/m^2) compare to the 15 ppm Pt loading (312 mmol/m^2). This result is similar when 24 ppm Pt

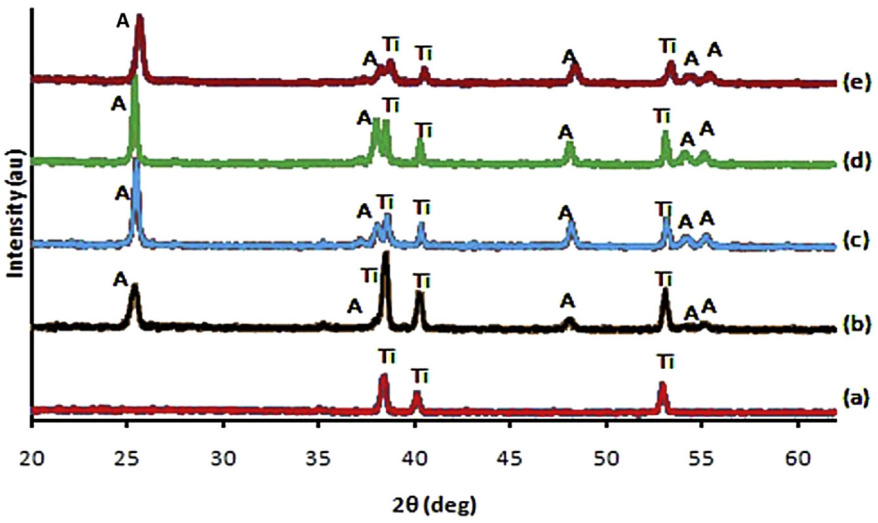

Fig. 6 – XRD pattern of photocatalysts (a) amorphous TNTA, (b) TNTA, (c) Pt-TNTA-PDC, (d) Pt-TNTA-CRA, and (e) Pt-TNTA-CRC.

Please cite this article in press as: Slamet, et al., Enhanced photocatalytic activity of Pt deposited on titania nanotube arrays for the hydrogen production with glycerol as a sacrificial agent, International Journal of Hydrogen Energy (2017), http://dx.doi.org/10.1016/j.ijhydene.2017.07.208

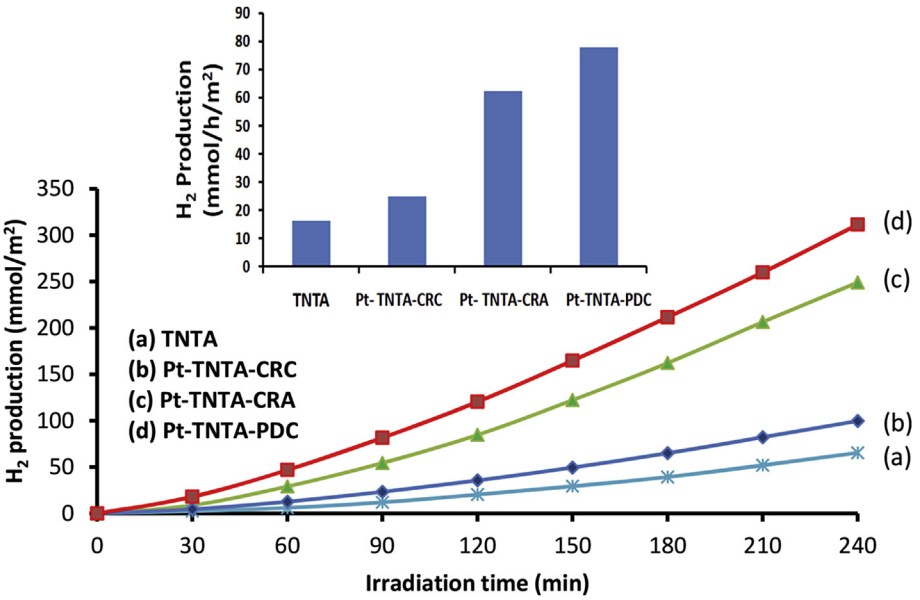

Fig. 7 – Accumulative H_2 generation as a function of irradiation time for various photocatalyst. The inset performs H_2 production rate as a function of variety of photocatalysts.

loading on TNTA via chemical reduction method was performed and it has been reported above (Fig. 1). Hereafter, 15 ppm of Pt loading on TNTA via photo-assisted deposition method was used as the photocatalyst in studying product identification and reaction pathway.

Identification of the final and intermediate product and prediction of reaction pathway

According to the identification, the final gas products of glycerol photo reforming are H_2, CO_2, and O_2. The existence of the CO_2 gave an evident that glycerol, as a sacrificial agent, underwent photo reforming reaction, whereas the presence of O_2 indicated that water splitting also occurred. Thus, it is obvious that glycerol acts as a sacrificial agent that reacts with the hole to produce H_2. The present of an organic additive can enhance H_2 production since it plays an effective as the reactant as well as the sacrificial agent that reduce the recombination [6,45]. The rate of H_2 formation from glycerol photo reformation is faster than water splitting since hole efficiently reacts with organic additive glycerol that inhibits recombination of electron-hole pairs [13,14]. The H_2 and CO_2 produced by photo-reforming of glycerol solution can be seen in Fig. 8.

From Fig. 8, it is obvious that irradiation time up to 240 min, the formation of H_2 and CO_2 increased. Up to 90 min irradiation, the mole ratio of H_2:CO_2 almost constant with 7:3 or 2.33 according to the reaction stoichiometry (Eq. (4)). However, after 90 min irradiation, the mole ratio became smaller than 2.33 (Fig. 8 inset), meant that there was the excess CO_2 produced. Moreover, H_2 produced also from water splitting. This excess of CO_2 is predicted come from photo-oxidation of glycerol with O_2 in the solution (the result of water splitting) that simultaneously taken place with photo-reformation glycerol as follows [10,11,13,15]:

$$C_3H_8O_3 + 3H_2O \rightarrow 3CO_2 + 7H_2 \text{ (photo-reformation)} \quad (4)$$

$$C_3H_8O_3 + (7/2)O_2 \rightarrow 3CO_2 + 4H_2O \text{ (photo-oxidation)} \quad (5)$$

Some of the intermediate products are identified in the gas phase (ethylene glycol, methanol, formaldehyde, acetone, acetic acid, and ethanol) and in the liquid phase (ethylene glycol and acetic acid). The total amount (gas and liquid) of intermediate products (except methanol that only in the small amount) are shown in Fig. 9. Methanol is also intermediate product obtained from glycerol photo-reforming using CuO_x-TiO_2 [11]. A number of intermediate products in the liquid phase indicates that those products are adsorbed on the surface of the photocatalyst, and some of them are desorbed to make a further reaction. It is observed that the dominant intermediate products are ethylene glycol and acetic acid. From Fig. 9, the total amount of all intermediate products ascend with the increasing time of irradiation and then diminish periodically. Diminishing the intermediate products meant that they converted to the next intermediates and eventually changed to the final products. Some intermediate products identified in the glycerol reforming by previous researchers is shown in Table 1 and ethylene glycol is an intermediate product that only detected in this study.

To study the effect of Pt deposited on TNTA, the analysis of intermediate products also performed for the glycerol photo-reforming with bare TNTA. The result indicated that intermediate products detected in the gas phase were ethylene glycol with the concentration smaller than in the Pt-TNTA-PDC (data not presented). It gave an indication that the activity of Pt-TNTA-PDC is better since the role of Pt as an electron trapper that reduces the recombination of electron-hole pairs. At the certain time, if the rate of H_2 production is

Please cite this article in press as: Slamet, et al., Enhanced photocatalytic activity of Pt deposited on titania nanotube arrays for the hydrogen production with glycerol as a sacrificial agent, International Journal of Hydrogen Energy (2017), http://dx.doi.org/10.1016/j.ijhydene.2017.07.208

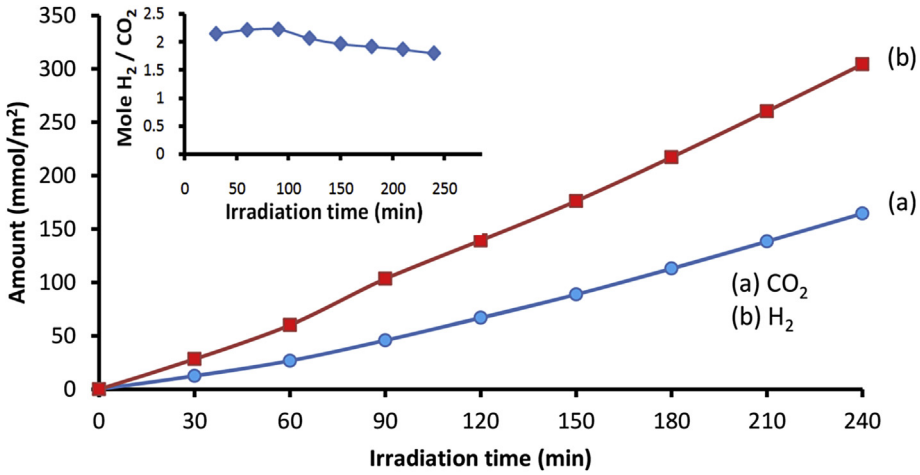

Fig. 8 – The H_2 and CO_2 generated by Pt-TNTA-PDC as a function of irradiation time. Inset is the comparison of H_2:CO_2 production vs irradiation time.

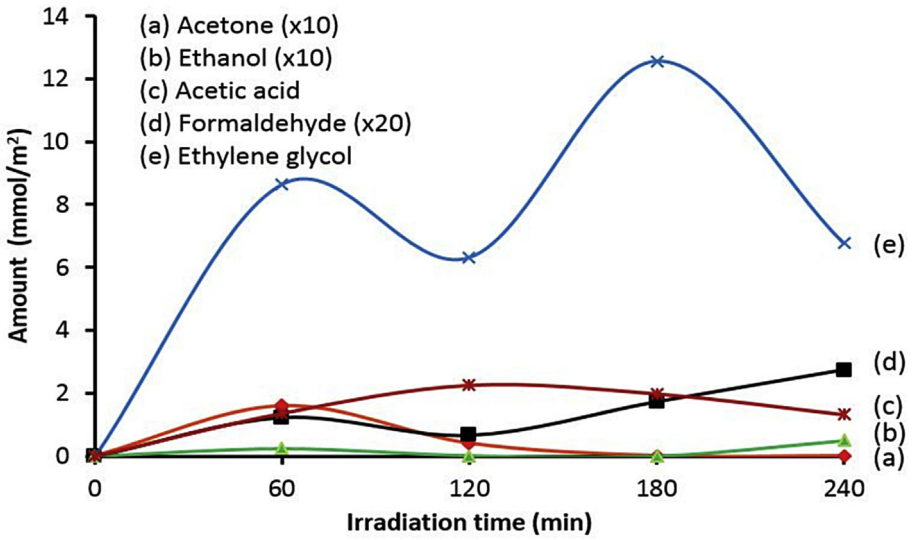

Fig. 9 – The total amount of some intermediate products detected as a function of irradiation time with Pt-TNTA-PDC.

Table 1 – Some intermediate products from glycerol reformation.

Photocatalysts	Intermediate products	Researchers
Pt/B/N $TiO_2$and Pt/TiO_2	Gas phase: methanol, methane, ethane and CO (trace element). Liquid phase: acetone.	Luo et al. [46]
Pt/TiO_2 P25	Liquid phase: glyceraldehyde, glycolaldehyde, glycolic acid, dan formaldehyde.	Li et al. [47]
Pt/TiO_2P25	Liquid phase: methanol and acetic acid	Daskalaki VM and Kondarides DI [14]
Pt/TiO_2P25	Liquid phase: acetol, acetaldehyde, ethanol, methanol. In small amount: glyceraldehydes, glycoaldehyde, acetone and acreoline	Panagiotopoulou et al. [13]
Pt/TNTA	Gas phase: ethylene glycol, methanol, formaldehyde, acetone, acetic acid and ethanol. Liquid phase: ethylene glycol and acetic acid	This study

Please cite this article in press as: Slamet, et al., Enhanced photocatalytic activity of Pt deposited on titania nanotube arrays for the hydrogen production with glycerol as a sacrificial agent, International Journal of Hydrogen Energy (2017), http://dx.doi.org/10.1016/j.ijhydene.2017.07.208

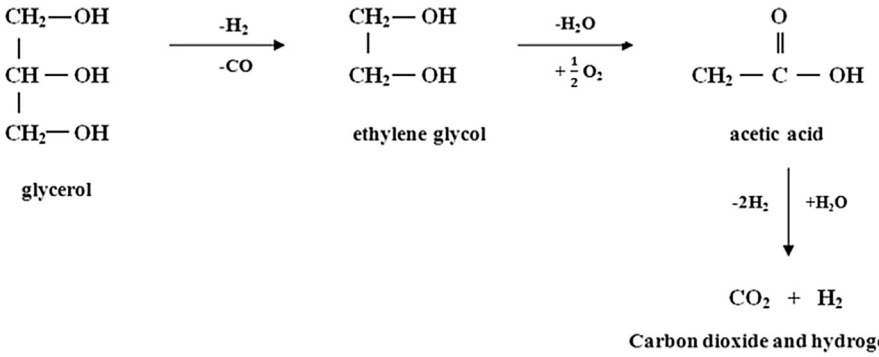

Fig. 10 – Proposed reaction pathway of glycerol-photo reforming over Pt-TNTA-PDC.

higher, results in higher rate of intermediate product as well. A similar result is also reported by Panagiotopoulou et al. [13].

The intermediate products detected in this study (ethylene glycol, methanol, formaldehyde, acetone, acetic acid and ethanol) are partly present in the pathway proposed by Panagiotopoulou et al. [13]. Therefore, this study supported the mechanism suggested by them. However, ethylene glycol is an intermediate product that has not been founded yet by formerly researchers. Since ethylene glycol and acetic acid are always present in the two phases, the prediction mechanism is glycerol underwent dehydrogenation become glyceraldehyde and followed by decarbonylation reaction, which leads to the formation of ethylene glycol and it experiences the dehydration and oxidation reactions to form acetic acid. Dehydrogenation of acetic to formed CO and it is transformed to CO_2 and H_2 via water-gas shift reaction [48]. Besides enhancing the rate of reaction, the role of Pt gave direction that the proposed reaction pathway is: glycerol → ethylene glycol → acetic acid → H_2 and CO_2. Fig. 10 presents the proposed reaction pathway.

Conclusions

Pt-decorated TiO_2 nanotube arrays (Pt-TNTA) have been successfully synthesized via anodization of Ti foils, which was followed by deposition of Pt nanoparticles. Two different deposition techniques are presented, namely chemical reduction using a strong reducing agent ($NaBH_4$) and photo-assisted deposition. Decorating Pt on TNTA did not affect the nanotubular structure of TNTA, while narrowed band gap was observed. The presence of Pt nanoparticles is essential to achieve effective H_2 photocatalytic production, as they offer an electron-trapping feature for better electron-hole separation. Pt loading which gave the best performance of H_2 photoproduction was obtained when photo-assisted deposition method (Pt-TNTA-PDC) is applied with Pt salt concentration of 15 ppm in the solution. The beneficial effect of glycerol as a sacrificial agent is attributable to the hole-scavenging feature it offers. Identification of CO_2 in the final product confirms the effectiveness of glycerol in quenching the photo-generated holes, which constitutes higher H_2 yield. Furthermore, corroborated by the identified intermediate products, the mechanism and the manner in which glycerol is consumed is proposed in the present study. On the basis of our findings, we also suggest that the role of Pt was not confined in recombination inhibition, but it could also direct the reaction route of glycerol photo-reforming.

Acknowledgments

The authors would like to thank LP3M Institut Teknologi Indonesia and Directorate General of Higher Education (DGHE), Indonesian Ministry of National Education for the financial support of this research (Hibah Bersaing grant no. 025/K3/KM/SPK/2013). Thank also to Muhammad Ibadurrohman for the contribution in this paper.

REFERENCES

[1] Gao H, Zhang P, Hu J, Pan J, Fan J, Shao G. One-dimensional Z-scheme TiO_2/WO_3/Pt heterostructures for enhanced hydrogen generation. Appl Surf Sci 2017;391:211–7.
[2] Li C, Yuan J, Han B, Jiang L, Shangguan W. TiO_2 nanotubes incorporated with CdS for photocatalytic hydrogen production from splitting of water under visible light irradiation. Int J Hydrogen Energy 2010;35:7073–9.
[3] Pei F, Liu Y, Xu S, Lu J, Wang C, Cao S. Nanocomposite of graphene oxide with nitrogen-doped TiO_2 exhibiting enhanced photocatalytic efficiency for hydrogen evolution. Int J Hydrogen Energy 2013;38:2670–7.
[4] Wu H, Zhang Z. High photoelectrochemical water splitting performance on nitrogen doped double wall TiO_2 nanotube arrays electrode. Int J Hydrogen Energy 2011;36:13481–7.
[5] Anthony RP, Mathews T, Ramesh C, Murugesan N, Dasgupta D, Dhara S, et al. Efficient photocatalytic hydrogen generation by Pt modified TiO_2 nanotubes fabricated by rapid breakdown anodization. Int J Hydrogen Energy 2012;37:8268–76.
[6] Ratnawati, Gunlazuardi J, Dewi EL, Slamet. Effect of $NaBF_4$ addition on the anodic synthesis of TiO_2 nanotube arrays photocatalyst for hydrogen production from glycerol solution. Int J Hydrogen Energy 2014;39:16927–35.
[7] Hakamizadeh M, Afshar S, Tadjarodi A, Khajavian R, Fadaie MR, Bozorgi B. Improving hydrogen production via water splitting over Pt/TiO_2/activated carbon nanocomposite. Int J Hydrogen Energy 2014;39:7262–9.

Please cite this article in press as: Slamet, et al., Enhanced photocatalytic activity of Pt deposited on titania nanotube arrays for the hydrogen production with glycerol as a sacrificial agent, International Journal of Hydrogen Energy (2017), http://dx.doi.org/10.1016/j.ijhydene.2017.07.208

[8] Melian EP, Lopez CR, Mendez AO, Diaz OG, Suarez MN, Rodriguez JMD, et al. Hydrogen production using Pt-loaded TiO_2 photocatalysts. Int J Hydrogen Energy 2013;38:11737–48.
[9] Ma BJ, Kim JS, Choi CH, Woo SI. Enhanced hydrogen generation from methanol aqueous solutions over Pt/MoO_3/TiO_2 under ultraviolet light. Int J Hydrogen Energy 2013;38:3582–7.
[10] Cargnello M, Gasparotto A, Gombac V, Montini T, Barreca D, Fornasiero P. Photocatalytic H_2 and added-value by-products – the role of metal oxide Systems in their synthesis from oxygenates. Eur J Inorg Chem 2011:4309–23.
[11] Gombac V, Sordelli L, Montini T, Delgado JJ, Adami G, Adamski A, et al. CuO_x-TiO_2 photocatalysts for H_2 production from ethanol and glycerol solutions. J Phys Chem A 2010;114:3916–25.
[12] Montini T, Gombac V, Sordelli L, Delgado JJ, Chen X, Adami G, et al. Nanostructured Cu/TiO_2 photocatalysts for H_2 production from ethanol and glycerol aqueous solutions. Chem Catal Chem 2011;3:574–7.
[13] Panagiotopoulou P, Karamerou EE, Kondarides DI. Kinetics and mechanism of glycerol photo-oxidation and photo-reforming reaction in aqueous TiO_2 and Pt/TiO_2 suspensions. Catal Today 2013;209:91–8.
[14] Daskalaki VM, Kondarides DI. Efficient production of hydrogen by photo-induced reforming of glycerol at ambient conditions. Catal Today 2009;144:75–80.
[15] Li F, Gu Q, Niu Y, Wang R, Tong Y, Zhu S, et al. Hydrogen evolution from aqueous-phase photocatalytic reforming of ethylene glycol over Pt/TiO_2 catalysts: role of Pt and product distribution. Appl Surf Sci 2017;391:251–8.
[16] Liu Y, Wang Z, Huang W. Influences of TiO_2 phase structures on the structures and photocatalytic hydrogen production of CuOx/TiO_2 photocatalysts. Appl Surf Sci 2016;389:760–7.
[17] Wang X, Shengsen Z, Xie Y, Wang H, Yu H, Shen, et al. Branched hydrogenated TiO_2 nanorod arrays for improving photocatalytic hydrogen evolution performance under simulated solar light. Int J Hydrogen Energy 2016;41:1–6.
[18] Xu F, Xiao W, Cheng B, Yu J. Direct Z-scheme anatase/rutile bi-phase nanocomposite TiO_2 nanofiber photocatalyst with enhanced photocatalytic H_2-production activity. Int J Hydrogen Energy 2014;39:15394–402.
[19] Lei P, Wang P, Gao X, Ding Y, Zhang S, Zhao J, et al. Immobilization of TiO_2 nanoparticles in polymeric substrates by chemical bonding for multi-cycle photodegradation of organic pollutants. J Hazard Mater 2012;227–228:185–94.
[20] Zhang L, Pan N, Lin S. Influence of Pt deposition on water splitting hydrogen generation by highly-ordered TiO_2 nanotube arrays. Int J Hydrogen Energy 2014;39:13474–80.
[21] Zhang C, Yu H, Li Y, Fu L, Gaao Y, Song W, et al. Simple synthesis of Pt/TiO_2 nanotube arrays with high activity and stability. J Electroanal Chem 2013;701:14–9.
[22] Carp O, Huisman CL, Reller A. Photoinduced reactivity of titanium dioxide. Prog Solid State Chem 2004;32:33–177.
[23] Robertson PKJ, Robertson JMC, Bahnemann DW. Removal of microorganisms and their chemical metabolites from water using semiconductor photocatalysis. J Hazard Mater 2012;211–212:161–71.
[24] Fujishima A, Zhang X, Tryk DA. TiO_2 photocatalysis and related surface phenomena. Surf Sci Rep 2008;63:515–82.
[25] Zhu Y, Chen Z, Gao T, Huang Q, Niu F, Qin L, et al. Construction of hybrid Z-scheme Pt/CdS-TNTAs with enhanced visible-light photocatalytic performance. Appl Catal B Environ 2015;163:16–22.
[26] Muhamed AER, Rohani S. Modified TiO_2 nanotube arrays (TNTAs): progressive strategies towards visible light responsive photoanode, a review. Energy Environ Sci 2011;4:1065–86.
[27] Zhu Z, Wang Y, Chen Z, Qin L, Yang L, Zhu L, et al. Visible light induced photocatalysis on CdS quantum dots decorated TiO_2 nanotubes arrays. Appl Catal A General 2015;498:159–66.
[28] An H, Zhou J, Li J, Zhu B, Wang S, Zhang S, et al. Deposition of Pt on the stable TiO_2 and its photocatalytic performance. Catal Commun 2009;11:175–9.
[29] Khan MA, Akhtar MS, Wo SI, Yang OB. Enhanced photoresponse under visible light in Pt ionized TiO_2 nanotube for the photocatalytic splitting of water. Catal Commun 2008;10:1–5.
[30] Meng A, Zhang J, Xu D, Cheng B, Yu J. Enhanced photocatalytic H_2-production activity of anatase TiO_2 nanosheet by selectively depositing dual-cocatalysts on {101} and {001} facets. Appl Catal B Environ 2016;198:286–94.
[31] He Z, Fu J, Cheng B, Yu J, Cao S. $Cu_2(OH)_2CO_3$ clusters: novel noble-metal-free cocatalysts for efficient photocatalytic hydrogen production from water splitting. Appl Catal B Environ 2017;205:104–11.
[32] Hassan FMB, Nanjo H, Venkatachalam S, Kanakubo M, Ebina T. Functionalization of electrochemically prepared titania nanotubes with Pt for application as catalyst for fuel cells. J Power Sources 2010;195:5889–95.
[33] Van MN, Li W, Sheng P, Van HP, Cai Q. Photoelectrochemical label-free immunoassay of octachlorostyrene based on heterogeneous CdSe/CdS/Pt/TiO_2 nanotube array. J Electroanal Chem 2015;736:69–75.
[34] Xing L, Jia J, Wang Y, Zhang B, Dong S. Pt modified TiO_2 nanotubes electrode: preparation and electrocatalytic application for methanol oxidation. Int J Hydrogen Energy 2010;35:12169–73.
[35] Yi H, Peng T, Ke D, Zan L, Yan C. P Photocatalytic H_2 production from methanol aqueous solution over titania nanoparticles with mesostructures. Int J Hydrogen Energy 2008;33:672–8.
[36] Slamet, Tristantini D, Valentina, Ibadurrahman M. Photocatalytic hydrogen production from glycerol-water mixture over Pt-N-TiO_2 nanotube photocatalyst. Int J Energy Res 2013;37:1372–81.
[37] Ratnawati, Gunlazuardi J, Slamet. Synthesis of titania nanotubes arrays by sonication aided anodization and its application for hydrogen generation from aqueous glycerol solution. Matec Web Conf 2015;28:01001.
[38] Zhou L, Deng J, Zhao Y, Liu W, An L, Chen F. Preparation and characterization of N-I Co-doped nanocrystal anatase TiO_2 with enhanced photocatalytic activity under visible-light irradiation. Mater Chem Phys 2009;117:522–7.
[39] Yu J, Dai G, Cheng B. Effect of crystalization methods on morphology and photocatalytic activity of anodized TiO_2 nanotube array film. J Phys Chem C 2010;117:19378–85.
[40] Ratnawati, Gunlazuardi J, Slamet. Development of titania nanotube arrays: the roles of water content and annealing atmosphere. Mater Chem Phys 2015;160:111–8.
[41] Slamet, Anny, Setiadi. Photocatalytic hydrogen generation from glycerol and water using Pt-loaded N–doped TiO_2 nanotube. Int J Eng Tech 2012;12:47–53.
[42] Stengl V, Bakardjieva S, Murafa N. Preparation and photocatalytic activity of rare earth doped TiO_2 nanoparticles. Mater Chem Phys 2009;114:217–26.
[43] Ahmed LM, Ivanova I, Hussein FH, Bahnemann DW. Role of platinum deposited on TiO_2 in photocatalytic methanol oxidation and dehydrogenation reactions. Int J Photoenergy 2014, 503516. 9 pages.
[44] Job N, Lambert S, Chatenet CJ, Gommes CJ, Maillard F, Fabry SB, et al. Preparation of highly loaded Pt/carbon xerogel catalysts for proton exchange membrane fuel cells by the strong electrostatic adsorption method. Catal Today 2010;150:119–27.

Please cite this article in press as: Slamet, et al., Enhanced photocatalytic activity of Pt deposited on titania nanotube arrays for the hydrogen production with glycerol as a sacrificial agent, International Journal of Hydrogen Energy (2017), http://dx.doi.org/10.1016/j.ijhydene.2017.07.208

[45] Wei LF, Zheng XJ, Zhang ZH, Wei YJ, Xie B, Wei MB, et al. A systematic study of photocatalytic H_2 production from propionic acid solution over Pt/TiO_2 photocatalyst. Int J Energy Res 2012;36:75–86.
[46] Luo N, Jiang Z, Shi H, Cao F, Xiao T. Photo-catalytic conversion of oxygenated hydrocarbons to hydrogen over heteroatom-doped TiO_2 catalysts. Int J Hydrogen Energy 2009;34:125–9.
[47] Li M, Li Y, Peng S, Lu G, Li S. Photocatalytic hydrogen generation using glycerol wastewater over Pt/TiO_2. Front Chem China 2009;4:32–8.
[48] Bahruji H, Bowker M, Davies PR, Pedrono F. New insights into the mechanism of photocatalytic reforming on Pd/Ti O_2. Appl Catal B Environ 2011;107:205–9.

Please cite this article in press as: Slamet, et al., Enhanced photocatalytic activity of Pt deposited on titania nanotube arrays for the hydrogen production with glycerol as a sacrificial agent, International Journal of Hydrogen Energy (2017), http://dx.doi.org/10.1016/j.ijhydene.2017.07.208